applied sciences

MDPI

Article

Vibration Characterization and Fault Diagnosis of a Planetary Gearbox with a Wireless Embedded Sensor

Li-Te Huang [1,2] and Jen-Yuan Chang [2,3,*]

[1] Mechanical and Mechatronics Systems Research Labs, Industrial Technology Research Institute, Chutung, Hsinchu 31057, Taiwan
[2] Department of Power Mechanical Engineering, National Tsing Hua University, Hsinchu 30013, Taiwan
[3] Mechanical & Computer-Aided Engineering, National Formosa University, Huwei, Yulin 632, Taiwan
* Correspondence: jychang@pme.nthu.edu.tw; Tel.: +886-3-594-2498

Abstract: A planetary gearbox is more complex in structure and motion than a gearbox with a fixed shaft, making it difficult to monitor and make a fault diagnosis in practice. Components must be frequently inspected to avoid excessive wear, but there is no simple way to directly measure wear. The most direct method is to log vibration and temperature signals using external sensors. Wireless sensors offer more space advantages than a wired one, so this study developed a measurement system that features a three-axis MEMS accelerometer, temperature sensing and wireless modules that are integrated into a planetary gearbox. Along with the system, a virtual instrument (VI) utilizing graphics programming language LabVIEW was developed to acquire and display data time and frequency domains to detect the gear's faults. To determine the root cause of vibrations in a planetary gearbox, determine the vibration signal model of amplitude modulation (AM) and frequency modulation (FM) due to gear damage and derive the characteristic frequencies of vibrations for a planetary gearbox, the characteristic frequencies and AMFM modulation were summarized in closed form. Different degrees of each gear damage were then detected in the planetary gearbox. The vibration signal model was validated by experiments to indicate the sideband around the gear meshing frequency and its feasibility for fault diagnosis of a planetary gearbox with the wireless embedded sensor.

Keywords: planetary gearbox; wireless sensor; virtual instrumentation; mechanical wear; vibration

Citation: Huang, L.-T.; Chang, J.-Y. Vibration Characterization and Fault Diagnosis of a Planetary Gearbox with a Wireless Embedded Sensor. *Appl. Sci.* **2023**, *13*, 729. https://doi.org/10.3390/app13020729

Academic Editors: Chun-Yen Chang, Charles Tijus, Teen-Hang Meen and Po-Lei Lee

Received: 2 December 2022
Revised: 25 December 2022
Accepted: 3 January 2023
Published: 4 January 2023

1. Introduction

As the manufacturing machine tool industry demands high transmission performance, this pushes a planetary transmission system to offer greater precision, torque density, efficiency and load capacity than a gearbox with a fixed-shaft format, in particular in the cases when heavy loads occur, or high precision is required. The gearbox includes gears, shafts and bearings, which are susceptible to wear and impact damage [1,2]. A failure of the gearbox can stop a process and result in major economic losses. Regular maintenance checks using an external sensor such as an accelerometer are commonly used in the industry for sanity checks and diagnosis of performance, but the limitations of machine installations and transmission distance requirements indicate that embedded and wireless sensors are required.

Advances in MEMS (micro-electro-mechanical system) technology allow smaller and lighter inertial sensors pushing their natural frequencies to a higher spectrum so as to be decoupled from the measured system's natural frequencies. MEMS sensors feature low quality, low power consumption, small size and integration with control and sensing electronics so they are ideal for applications when space is a critical issue. A MEMS sensor also allows wireless communication. Several wireless sensor systems [3–7] have been proposed to estimate the wear of mechanical components using MEMS technology. These

studies use wireless sensors to measure wear, to design signal processing tools, to reduce energy losses and to increase signal accuracy.

One study [3] collected signals from a ball screw to estimate the state of wear. The sensing components were attached to the surface of a gearbox and a machine tool. Hou and Bergmann [4] measured the structural variations in the dynamic mode where continuous signals have been used to determine the state of an induction motor. Other studies, Refs. [5,6], developed wireless sensor systems to transfer data to a data server for analysis. A previous study [7] collected vibration signals from sensors that were mounted on wind turbines, and the experimental results verified the effectiveness of the gearbox fault diagnosis. Other studies [3–7] designed wireless sensors for industrial environments, using vibration results to determine the life of rotating parts and dynamic power management techniques to extend the life of a system.

Signals such as preload, temperature and vibrations can certainly be transmitted wirelessly and used to detect the working status of mechanical parts, from which the service life of mechanical parts can be estimated. However, most sensors are externally mounted and are not integrated in the transmission mechanism, so sensor life is shortened, and they are inconvenient to use. This study embeds a sensor in a transmission mechanism to detect vibration and temperature signals and extend the life of a transmission mechanism.

A virtual instrument (VI) is designed using the graphical programming language LabVIEW to acquire data, analyze the time and frequency domain and to ensure that data are persistent, archived and controlled. Wang and Gao [8] implemented LabVIEW using VI graphical language to monitor the condition of integrated bearings. Another study [9], to diagnose typical faults in a planetary gearbox, developed a VI system that simulated broken teeth on a sun gear using an envelope analysis. Another study [10] developed a system to remotely monitor the condition of a wind turbine gearbox and diagnose faults using MATLAB and LabVIEW to improve performance and speed. A previous study [11] used wavelet transformation and ensemble empirical mode decomposition to gather information about faults using a diagnosis technology that was developed using LabVIEW. Studies show that MEMS and LabVIEW are eminently suited to system monitoring and fault diagnosis.

A frequency spectrum analysis is used to determine the vibrational behavior of a planetary gearbox that is healthy or faulty [1,12]. Unlike fixed axis gearboxes, planetary gearboxes have compound rotary motion. The planet gears rotate on their own axis around the central sun gear. The sensor signal has amplitude modulation (AM) because the interfering positions of the sun gear meshing with planet gear and planet gear meshing with ring gear with respect to the sensor change over time, which is consistent with the findings of two studies [13,14]. The compound motion that is caused by multi-gear-meshing results in time variant vibration propagation paths, and this generates distinctive non-stationarity in the dynamic response for a planetary gearbox, so it is difficult to monitor the condition of a planetary gearbox. Characteristic frequencies directly reflect this mechanical modulation behavior, especially the sideband around the gear meshing frequency and its harmonics. The frequency and amplitude of these features vary for different operating conditions and types of gear damage, so the meshing frequency and sideband distribution that are produced by a planetary gearbox can be used to determine its state of wear.

McFadden and Smith [15], McNames [16] and Mosher [17] determined that the involute kinematics of planetary gearboxes produce complex and asymmetric sidebands in the vibration spectrum, which is in agreement with the results of another study [18]. Previous studies [15–18] did not simulate signals considering the effect of frequency modulation (FM). Inalpolat and Kahraman [19,20] developed a mathematical model to determine the effect of amplitude modulation (AM) and frequency modulation (FM) due to the rotation of the planet carrier and gear manufacturing errors in a dynamic model of a planetary gearbox, and they determined the sideband characteristics around meshing frequency harmonics. This improved dynamic model better predicted the sidebands in planetary gearboxes due to distributed gear errors.

Luo et al. [21] studied the amplitude modulation-based formula and used simple trigonometric function manipulations to determine the major physical phenomena in a planetary gearbox. This mathematical model determines the vibrational response for a planetary gearbox and is a reliable indicator of the condition of a planetary gearbox. He et al. [22] developed a mathematical model that considered the transmission path and the direction of the meshing force to determine the mechanisms for modulation sidebands. These studies predicted and explained sidebands more accurately, but they did not consider gear fault conditions in a planetary gearbox.

Feng and Zuo [23] constructed vibration signal models to diagnose faults in a planetary gearbox. The effect of amplitude modulation and frequency modulation due to gear damage and variations in the period of time working, and the effect of the vibration transfer path were determined using the results of previous studies [15–22]. The theoretical derivation was used to manually create and detect different degrees of local gear damage and naturally developed gear damage in a planetary gearbox. These frequency domain representations specifically demonstrated the presence of local cracks in the teeth of planetary gears, which are consistent with the results of another study [24].

A spectral analysis is used to diagnose transmission faults. The spectral structure of the vibration signal of a planetary gearbox and the failure symptoms of each gear are determined by a spectral analysis.

This study increases the robustness of gearbox systems in industrial applications. A planetary gearbox, an embedded sensor and a virtual instrument (as shown in Figure 1) are used to log the operating signal for mechanical parts. Considering the application limitations of installation, system integration and signal accuracy, this study constructs a verification test rig and artificially seeded faulty sun, planetary and ring gears to construct a frequency spectrum using the results of previous studies [15–24].

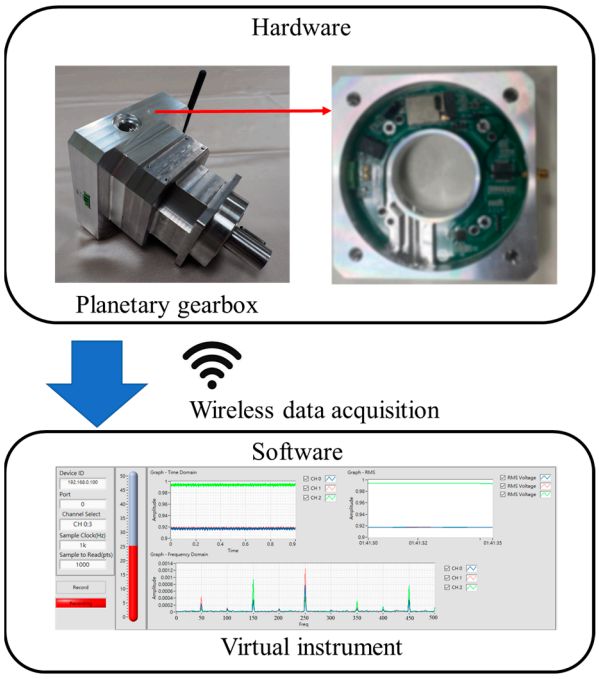

Figure 1. Gearbox with the proposed embedded sensor and VI system.

The contributions of this paper are as follows:

- To the authors' best knowledge, no industrial planetary gearboxes use embedded sensors with wireless transmission. Gearbox mechanics are determined using a surface-mounted accelerometer. This requires a greater installation space, stable accelerometer wires and complex signal reading. This study establishes the first wireless embedded

sensor in a gearbox to log mechanical signals and display them in a virtual instrument to allow Plug and Play for Internet of Things (IoT) applications.

- A printed circuit board is constructed that integrates temperature and vibration signals, transmits them to the server using a wireless module and uses LabVIEW to create a graphical interface. The signal is logged to analyze gearbox failure.
- Equations that describe the effect of amplitude modulation and frequency modulation (AMFM) due to gear damage and periodical changes in working conditions are derived.

Section 2 describes the measurement system's architecture and design. Section 3 presents the vibration signals for a planetary gearbox with gear damage and determines the effect of AM and FM and derives the corresponding Fourier transform in the frequency spectrum. Equations for calculating the characteristic frequency of each gear fault are derived in Section 4. Section 5 validates the vibration signal model using theoretical and industrial signal models to validate this analysis using experimental data sets for artificially seeded worn gear in the gearbox. Conclusions are detailed in Section 6.

2. Measurement System Architecture

This system analyzes the measurement data, which are used to predict the lifetime of the gearbox. A fast Fourier transform is applied to the vibration data to derive the vibration spectrum, which shows the condition of the gears.

The only gearbox with a data transmission function seen on the market is sold by Wittenstein (Igersheim, Germany). The product transmits temperature and vibration signals by wire using the IO-Link communication protocol. If the environment is limited in terms of space, a wired transmission method can be negatively affected, and without PLC or IO-Link hardware, it is impossible to receive data, so a printed circuit board with a wireless transmission function is embedded in the gearbox mechanism (as shown in Figure 2). The benefits over Wittenstein's product are described in the following.

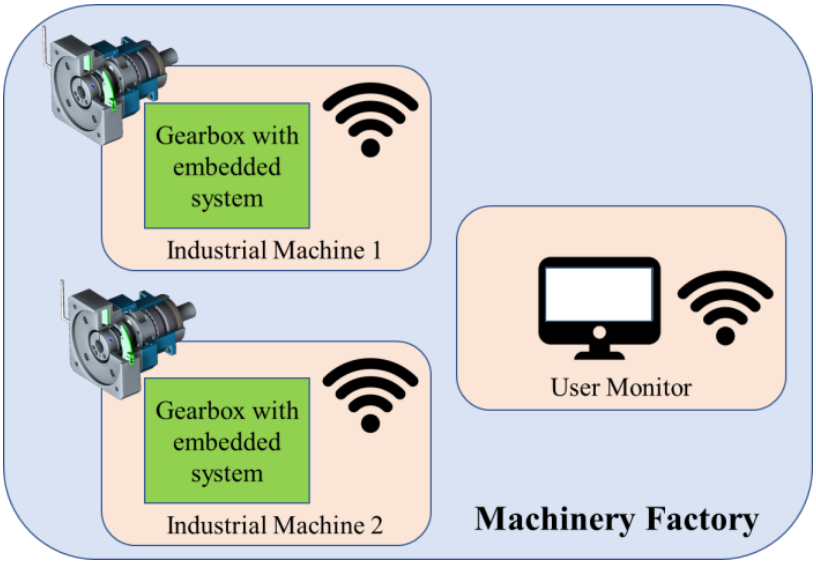

Figure 2. System architecture for the proposed gearbox.

- Wired transmission requires spatial limits. The embedded sensor is directly powered by the power source and can be used in a wide range of applications, regardless of environmental constraints.
- The measurement data are wirelessly transmitted to the user directly through this printed circuit board using the microcontroller and the wireless module, without the need for PLC or IO-Link hardware.

2.1. Development of Embedded Sensor Hardware

The measurement system for this study measures the three-axis vibration and gearbox temperature signals and sends these signals to a user's device by wireless communication. Figure 3 shows the general block diagram for the measurement system.

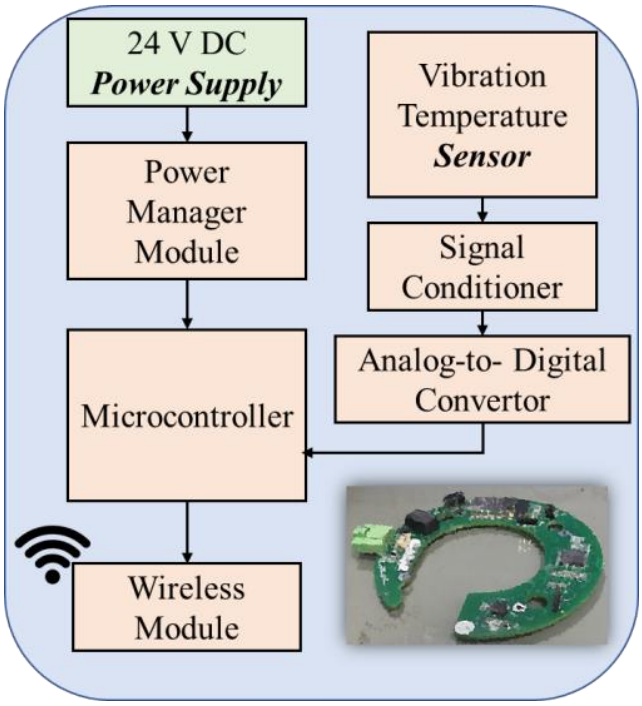

Figure 3. Operation flowchart and prototype of the embedded sensor.

To ensure that the measurement result is accurate, and the sensor is efficient, a signal conditioner is used to modify the signal, which is sent to a 16-bit analog convertor for digitalizing for the microcontroller. The microcontroller features logic to select a specific amount of data and transmit it using the wireless module.

- 24 VDC Power Module: Industrial environments use 24 VDC. Without the power management integrated circuit (PMIC), it is impossible to provide adequate power to the microcontroller; however, this module delivers sufficient power for the microcontroller.
- Microcontroller: A STM32 series microcontroller is used, which has an ARM Cortex-M3 core that meets all the necessary requirements for receiving sensor data and hardware communication. There are a total of 47 pins, including 10 analog input pins and 37 digital input and output pins, and the operating voltage is 2 to 3.6 VDC. The maximum clock speed is 72 MHz clock speed, and there are 128 Kbytes of flash memory and 20 Kbytes static random-access memory (SRAM). The microcontroller stores the sensor data values and sends these values to the receiver via a Wi-Fi module.
- Vibration Sensor: Figure 4 shows that the vibration sensor contains an accelerometer to record 3 axis (X, Y and Z) vibration data and a temperature sensor to measure the temperature of the gearbox. An amplifier and analog filter constitute preconditioning circuitry to amplify the acceleration of analog signals and filter them to suit the bandwidth of the sensor. A group of resistors and capacitors eliminate interference and noise.

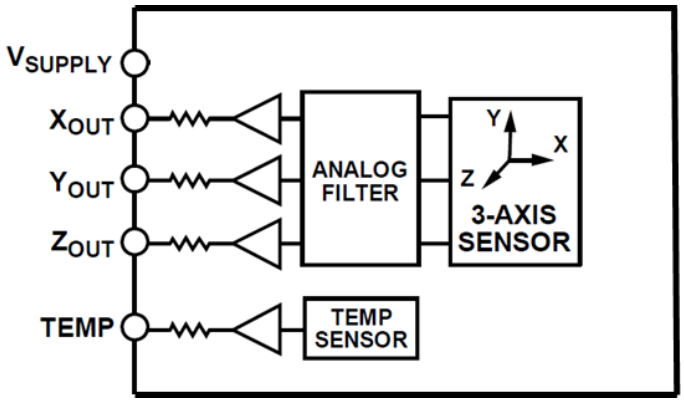

Figure 4. Block diagram of the vibration sensor.

- Wi-Fi Module: The Wi-Fi module includes an MCU and is used as a transmitter to send measurement data. It supports the standard IEEE 802.11 b/g/n protocol and a complete transmission control protocol/internet protocol (TCP/IP) stack. This module allows networking between devices and can be used to construct separate network controllers. The PCB and the monitoring system must be on the same local area network to transfer data.

The specification of the measurement system is detailed in Table 1. This specification can be changed for different applications, such as monitoring temperature at 1 Hz and vibration at 50–3000 Hz, as required by domain experts.

Table 1. Prototype specification.

System Specification		
Vibration Measurement	Channel number	3 axis
	Acceleration range	±10 g
	Sensitivity	80 mV/g
	Sampling rate	5 k Sps
	Resolution	16 bits
Temperature Measurement	Temperature range	−55~125 °C
	Measurement accuracy	±0.5 °C
	Sampling rate	5 Sps
Others	Input Power	24 V DC
	WiFi	802.11 standard protocol

2.2. Development of Embedded Sensor Software

This study uses LabVIEW to create a VI (virtual instrument) system that reads data and analyzes temperature and vibration signals. The program interface is user friendly, in terms of writing the program and building a user interface.

Figure 5 shows a flowchart for the various specific functions for the VI.

The VI system accepts two types of sensor signals, and measures vibration signals due to defects in the planetary gearbox structure. For a gear rotating at 7500 rpm, most defect-induced signals are distributed in the frequency band from 1.7 to 5000 Hz, as confirmed by analytical and experimental investigations. The signal also detects temperature variations within the planetary gearbox structure. These are typically low frequencies below 1 Hz. This study uses a multi-channel programmable data acquisition printed circuit board with a maximum sampling frequency of 10 kHz. The system samples signals from 0 to 5000 Hz without distortion.

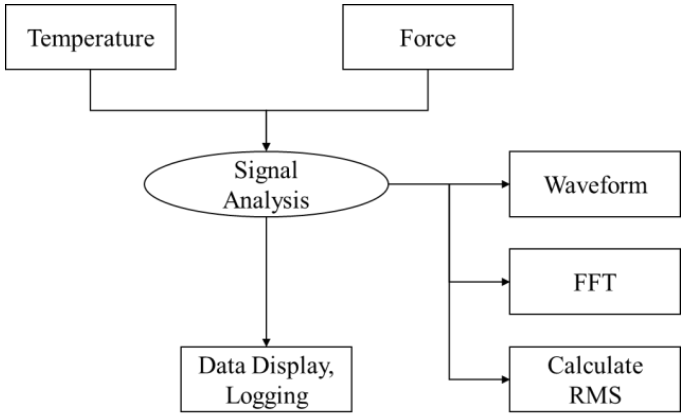

Figure 5. Flowchart for the VI.

A section of the VI main program is shown in Figure 6. Each module or icon in the diagram represents a function, such as data acquisition, signal display, spectrum display, Fourier transform analysis, calculation of root mean square values and data logging.

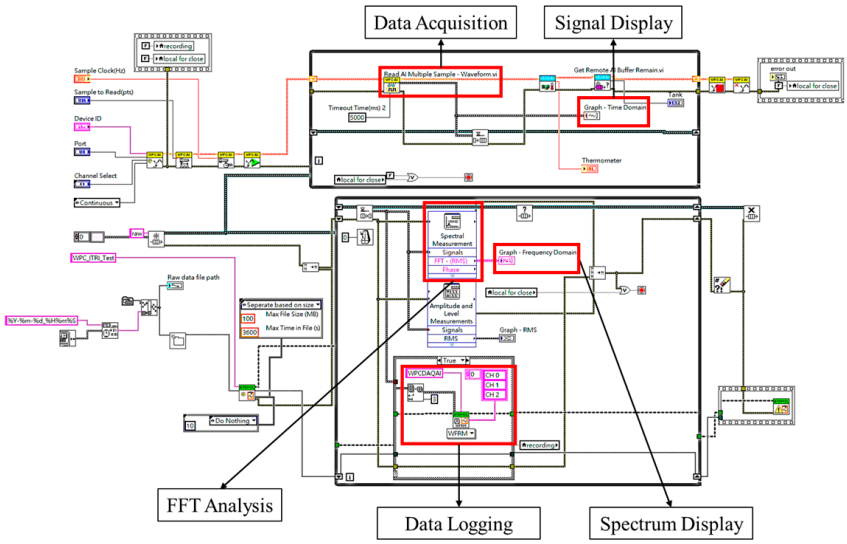

Figure 6. Main program details of the VI system.

The signal analysis module provides a time domain analysis, frequency analysis and calculates the root mean square for the vibration signal. The data are transferred to waveform data and shown in the time domain and are then processed using a Fourier transform to give a result in the frequency domain. The RMS result is calculated using these data. The raw data are logged into a file that contains three-axis acceleration data.

The VI must offer an explicit graphical user interface that allows an observer to efficiently communicate with the gear monitoring system. Figure 7 shows the graphical user interface. Depending on the frequency of the signal, anti-aliasing and sampling rates for different gear operation modes are adjusted. The waveform display window in the upper middle left part of the menu shows the time domain for real-time gear signals. The frequency display window at the bottom center of the menu shows the spectrum of the real-time response signal from the Fourier transform analysis. The remaining functions of the menu include a real-time temperature display, and a data logging trigger, which is clicked one time to start recording the raw data and once to stop recording.

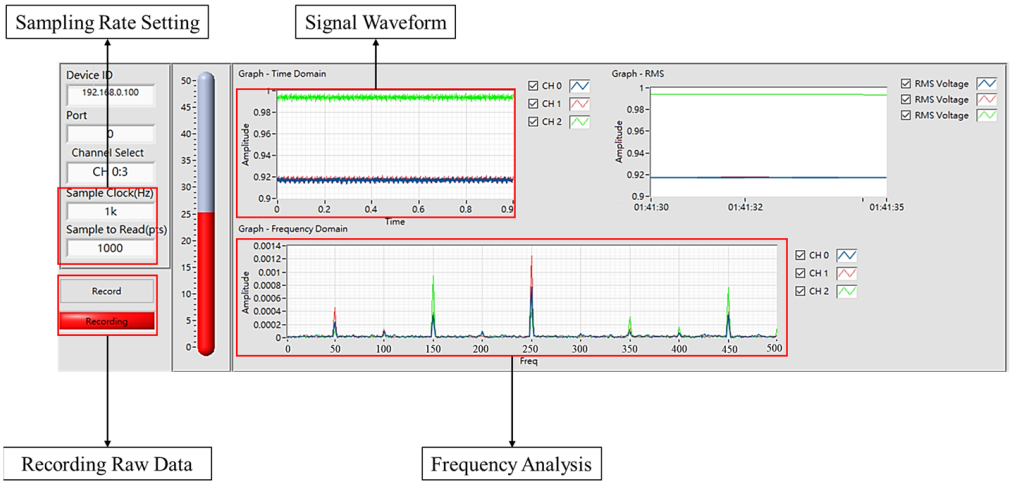

Figure 7. A graphical user interface showing signal waveform in time domain and the corresponding frequency spectrum.

To simulate interference in gearbox operation characteristic frequencies, LabVIEW's built-in noise and the sine wave simulation function are used. The sine wave has a frequency of 250 Hz and an amplitude of 5, and the noise factor has an amplitude of 10. Figure 8 shows that the simulation result is correct because the Fourier transform result for the sine wave with noise signal matches the frequency of 250 Hz. The result is quite close in the time domain to the real result. This tool produces simulated vibration signals that are similar to real signals.

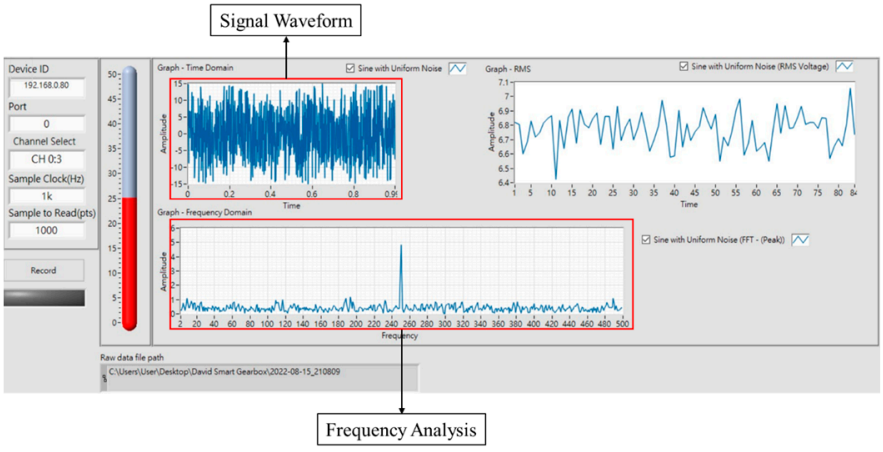

Figure 8. Graphical user interface results for a simulated sine wave with noise.

Using the Internet of Things (IoT), the vibration data are transmitted to the Internet database. A block diagram is shown in Figure 9.

The recording data are saved as a TDMS file, which is a file format that was created by National Instruments (NI) that is more efficient than Excel and can be used for a large amount of data. This type of file can be opened in either Excel or MATLAB.

Within the LabVIEW program, the System Exec.vi is used to call the uploading function script, which is written in Python. Nptdms, Pandas and Mysql-connector-python are three modules that are used for the script. Nptdms and Pandas are used to convert the TDMS file into a form that can be uploaded. Mysql-connector-python allows data to be uploaded to the Internet database that is maintained by SQL.

When the recording stops, the uploading button is used to run the script to upload the measurement data. There is a mechanism to ensure that the recording ends successfully

before uploading. The message can be viewed to ensure that the data are uploaded correctly to the Internet database.

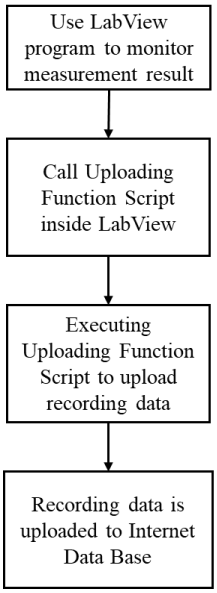

Figure 9. Block diagram for data upload.

This section describes the specifications of the developed PCB and the program architecture for LabVIEW. Vibration and temperature signals are transmitted via Wi-Fi to the PC for the real-time display, and the raw data are uploaded to the network database for further analysis.

3. Vibration Signal Model for a Planetary Gearbox

To address the problems of traditional sideband-related indicators, this study uses a typical planetary gear train. An illustrative configuration is shown in Figure 10. For a planetary gearbox, the ring gear is a fixed part, and the planet carrier and the planet gears are integrated together. In this study, r, p, s and H denote the ring gear, the planet gear, the sun gear and the planet carrier, respectively; N is the rotational speed; z is the number of gear teeth; and K is the number of planetary gears.

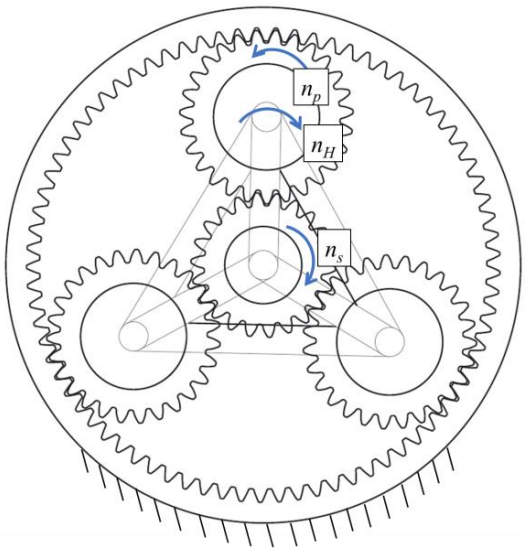

Figure 10. Schematic drawing of the planetary gear train.

The sun gear is fixed on the shaft as the high-speed input and the planet carrier is the low-speed output. The sensor is mounted on the fixed part to collect vibration data.

During the operation of the gearbox, the number of meshing teeth alternates with the rotation of the gear train. When there is tooth damage in the planetary gearbox, periodic pulses or severe modulations are produced in the vibration signal model with the characteristic frequency of the damage gear and the rotational frequency of the damage gear relative to the planet carrier, as described in a previous study [24].

Vibrational signals due to damage at the meshing site are modeled as amplitude modulation and frequency modulation (AMFM) processes to determine the impact of the vibrational signal. The effects of AM and FM due to cyclical changes in operating conditions are then measured.

When the damaged area meshes, the vibration signal at the meshing position is measured, excluding the effect of the transfer path on the vibration signal. The signal model is suitable for any gear system, whether it has a fixed-shaft gear or a planetary gear set. Gear meshing conditions change frequently due to errors in the manufacturing and assembly processes and gear failures. This damage creates a sudden change in the vibration signal while gear meshing. This causes amplitude modulation and frequency modulation in the original signal. Modulation is periodic and depends on the characteristic frequency of the damaged gear, so the AM and FM functions are expressed as a discrete Fourier series, for which the characteristic frequency of the damaged gear is the fundamental frequency. Therefore, the vibration signal model that is caused by the meshing of a faulty gear can be described in terms of amplitude and frequency modulation [23,24].

$$x_0(t) = \sum_{k=0}^{\infty} a_k(t) \cos[2\pi k f_m t + b_k(t) + \theta_k] \tag{1}$$

$$a_k(t) = A_0[1 + \sum_{n=1}^{\infty} A_{kn} \cos(2\pi n f_c t + \varphi_{kn})] \tag{2}$$

$$b_k(t) = \sum_{l=1}^{\infty} B_{kl} \sin(2\pi l f_c t + \phi_{kl}) \tag{3}$$

where $a_k(t)$ is the AM function; $b_k(t)$ is the FM function; $A_{kn} > 0$ is the AM magnitudes; $B_{kl} > 0$ is the FM magnitudes; A_0 is a dimensionless constant of the signal amplitude; f_m is the gear meshing frequency; f_c is the characteristic frequency; θ, φ and ϕ are the initial phases of AM and FM phases, respectively; N is the highest order of AM; and L is the highest order of FM to be considered.

For simplification, only the fundamental frequencies are used in (1) to (3), so only the case of $k = n = l = 1$ is considered. Therefore, (1) is simplified as:

$$x_0(t) = A_1[1 + A\cos(2\pi f_c t + \varphi_1)] \cdot \cos[2\pi f_m t + B\sin(2\pi f_c t + \phi_1) + \theta_1] \tag{4}$$

according to the identity

$$e^{jz\ \sin\varphi} = \sum_{k=-\infty}^{+\infty} J_k(z) e^{jk\varphi} \tag{5}$$

where $J_k(z)$ is a Bessel function of the first kind with integer order k and argument z, so (4) can be expanded as a sum of infinite harmonics:

$$x_0(t) = A_1[1 + A\cos(2\pi f_c t + \varphi_1)] \cdot \sum_{k=-\infty}^{+\infty} J_k(B) \cos[2\pi(f_m + k f_c)t + k\phi_1 + \theta_1] \tag{6}$$

Using the identities of trigonometric functions, (6) is rewritten as:

$$x_0(t) = \sum_{k=-\infty}^{+\infty} A_1 \cdot J_k(B)\Big\{\cos[2\pi(f_m + kf_c)t + \varphi_k] + \tfrac{A}{2}\cos[2\pi(f_m + kf_c + f_c)t + \phi_k] + \tfrac{A}{2}\cos[2\pi(f_m + kf_c - f_c)t + \theta_k]\Big\} \quad (7)$$

where f_c is the characteristic frequency, $\varphi_k = k\phi_1 + \theta_1$, $\phi_k = k\phi_1 + \varphi_1 + \theta_1$ and $\theta_k = -k\phi_1 + \varphi_1 - \theta_1$. A_1, $J_k(B)$ and A are constants, so (7) is simplified using the properties of trigonometric functions as:

$$x_0(t) = \sum_{k=-\infty}^{\infty} C_k \cos[2\pi(f_m + kf_c)t + \alpha_k] \quad (8)$$

where C_k and α_k are constants that are related to A_1, A, $\{J_i(B)\}$, $\{\varphi_i\}$, $\{\phi_i\}$ and $\{\theta_i\}$.

Equation (8) derives a series of sidebands for the damaged gear, with the spacing within the adjacent sidebands equal to the corresponding characteristic frequency for the faulty gear (f_c). In terms of harmonics, the nf_m ($n \in \mathrm{N}^*$) of the meshing frequency, the sidebands occur around the positions $nf_m \pm kf_c$ ($k \in Z$).

Equation (8) represents the vibration signal model for a fixed-shaft gear train transformed by a planetary gear train.

Sensor rotation causes amplitude modulation and frequency modulation in the vibration signal. This AM is modeled using a Hanning function [19,20]. For simplification, only the modulating phenomena inside the essential frequency are taken into consideration, and the vibration signal (t) is measured through the sensor and defined as:

$$x(t) = A_{H0}[1 + A_{H1}\cos(2\pi f_H t + \theta_H)]x_0(t) \quad (9)$$

where $x_0(t)$ is the original vibration signal represented by (8); and f_H is the relative rotation frequency of the sensor, which corresponds to the rotation frequency of the planet carrier; A_{H0} and A_{H1} are the signal attenuation coefficient and the strength of amplitude modulating, respectively.

Substituting (8) into (9) gives:

$$x(t) = \sum_{k=-\infty}^{\infty} D_k \cos[2\pi(f_m + kf_c \pm f_H)t + \beta_k] \quad (10)$$

where D_k and β_k ($k \in Z$) are the constants.

The effect of sensor rotation on the measured vibration signal is seen as spectral lines at $\pm f_H$ locations around sidebands $f_m \pm kf_c$ ($k \in Z$).

In terms of the harmonics of mesh frequency f_m, the modulation effects and harmonics of f_H, the sideband locations are $nf_m + kf_c + lf_H$ ($n \in \mathrm{N}^*$, $l \in Z$), where f_c is the characteristic frequency of one corresponding gear damage. For planetary gear sets, the configuration of the gearbox is the defining factor.

Section 4 discusses the calculation of the characteristic frequencies of a planetary gearbox. After a period of operation, gears become worn, and manufacturing and assembly errors affect the system, so there are some variations in the theoretical signal model.

4. Planetary Gear Train Meshing Frequency and Characteristic Frequencies

4.1. Gear Meshing Frequency

For local damage, the characteristic frequency of the damaged gear of the planetary gear is defined as the number of times damage occurs between the damaged gear tooth and the mating gear. This modulates the vibration of the mesh to the frequency of abrupt changes resulting from the mesh due to local gear damage.

For distributed damage, the characteristic frequency is defined as the relative number of rotations of the damaged gear to the planet carrier.

The meshing frequency between the planet gear and the ring gear is the same as the meshing frequency between the sun gear and the planet gear. For the planetary gearbox in Figure 10, the meshing frequency f_m is calculated as:

$$f_m = f_H \cdot z_r = \frac{z_r z_s}{z_r + z_s} \cdot f_{sh} \tag{11}$$

where f_{sh} is the sun gear's shaft rotation frequency.

4.2. Fault Sun Gear

For the local damage case, it is assumed that there is a single area of damage on a sun gear's tooth surface. The local fault meshes with the planet gear, so an impulse signal modulates the vibration signal. In one turn of the sun gear, modulation occurs K times. If these modulation states are exactly the same, the local fault (f_{csl}) of a sun gear is K times with the relative rotating frequency f_s^H:

$$f_{csl} = K \cdot f_s^H = K \cdot \frac{f_m}{z_s} = K \cdot \frac{z_r}{z_r + z_s} \cdot f_{sh} \tag{12}$$

For distributed damage on a sun gear, when the sun gear accomplishes one correlative turn, the change in the meshing state occurs in one period, so the matching characteristic frequency for the distributed fault (f_{csd}) of a sun gear is equal to the relative rotating frequency f_s^H:

$$f_{csd} = f_s^H = \frac{f_m}{z_s} = \frac{z_r}{z_r + z_s} \cdot f_{sh} \tag{13}$$

4.3. Fault Planet Gear

When local damage occurs on a planet gear tooth, the local damage engages the other gear, and the pulse signal modulates the vibration. Since this modulation phenomenon occurs only once in one revolution of the planet gear, the local disturbance (f_{cpl}) of the planet gear is equal to the relative rotating frequency f_p^H:

$$f_{cpl} = K \cdot f_p^H = K \cdot \frac{f_m}{z_p} = K \cdot \frac{z_r \cdot z_s}{z_p(z_r + z_s)} \cdot f_{sh} \tag{14}$$

If there is local damage on either side of the planet gear tooth, the damaged planet gear tooth will also mesh with other meshing gear and the vibration signal will be modulated twice during one rotation period. The planet gear with a two-sided local fault is twice the relative rotating frequency f_p^H:

$$f_{cpl} = 2f_p^H = 2 \cdot \frac{f_m}{z_p} = 2 \cdot \frac{z_r \cdot z_s}{z_p(z_r + z_s)} \cdot f_{sh} \tag{15}$$

For distributed damage on a planet gear, when the planet gear accomplishes one correlative turn, the change in the meshing state occurs in one period, so the matching characteristic frequency for the distributed fault (f_{cpd}) of a planet gear is equal to the relative rotating frequency of the planet gear f_p^H:

$$f_{cpd} = f_p^H = \frac{f_m}{z_p} = \frac{z_r \cdot z_s}{z_p(z_r + z_s)} \cdot f_{sh} \tag{16}$$

4.4. Fault Ring Gear

For local damage, the characteristic frequency for a faulty ring gear (f_{crl}) is:

$$f_{crl} = K \cdot \frac{z_s}{z_r + z_s} \cdot f_{sh} = K \cdot f_H \tag{17}$$

For distributed damage, the characteristic frequency for a faulty ring gear (f_{crd}) is:

$$f_{crd} = \frac{z_s}{z_r + z_s} \cdot f_{sh} = f_H \tag{18}$$

4.5. Analysis of the Simulated Signal

The number of teeth in the gearbox. the operating speed of the transmission and the characteristic frequency of fault gear are calculated using Equations (11)–(18) for local or distributed damage.

Gear faults are detected and located by examining the sideband structure and determining whether the sideband position is related to characteristic frequencies.

To verify this theoretical derivation and demonstrate the spectral structure of the vibration signal, two signals that simulate vibration caused by local damage to a planetary gear tooth are generated, one of which is calculated using (4). The other is calculated using (9) and includes the AM effect caused by the rotating planet carrier. The parameters for this simulation are listed in Table 2. The signal is sampled at a frequency of 500 Hz.

Table 2. Parameters for simulation.

AM Magnitude A	FM Magnitude B	f_m—Meshing Frequency (Hz)	f_H—Planet Carrier Rotating Frequency (Hz)	f_p^H—Fault Gear Characteristic Frequency (Hz)
1	0.5	216	2	4.6

If the waveform of the modulated signal is a sine wave, Figures 11 and 12 show the time domain waveform and the frequency spectrum. The spectral peaks are significantly larger at frequencies of $f_m \pm kf_p^H$, $(k \in Z)$ and other spectral lines are relatively small. This is consistent with the result of (7). The corresponding characteristic frequency of the planet gear with a local fault is $K \cdot f_p^H$, which is consistent with (14). The second signal includes the AM effect, so there are more spectral peaks as sidebands, when Figures 11 and 12 are compared. These sidebands are centered beside the mesh frequency and the rotation frequency of the planet carrier plus and minus the mesh frequency, which is $f_m \pm kf_p^H$ *and* $f_m \pm f_H \pm kf_p^H$, $(k \in Z)$. This behavior is consistent with the result using (10).

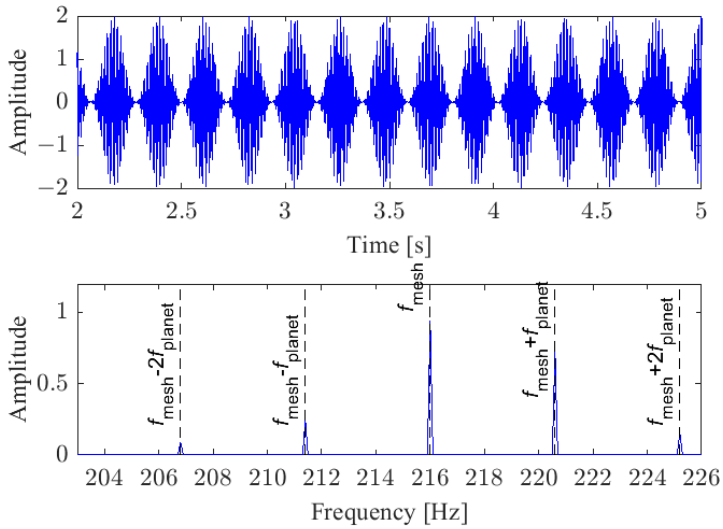

Figure 11. Simulated waveform and Fourier spectrum for a signal for planet gear damage, excluding the effect of the transfer path.

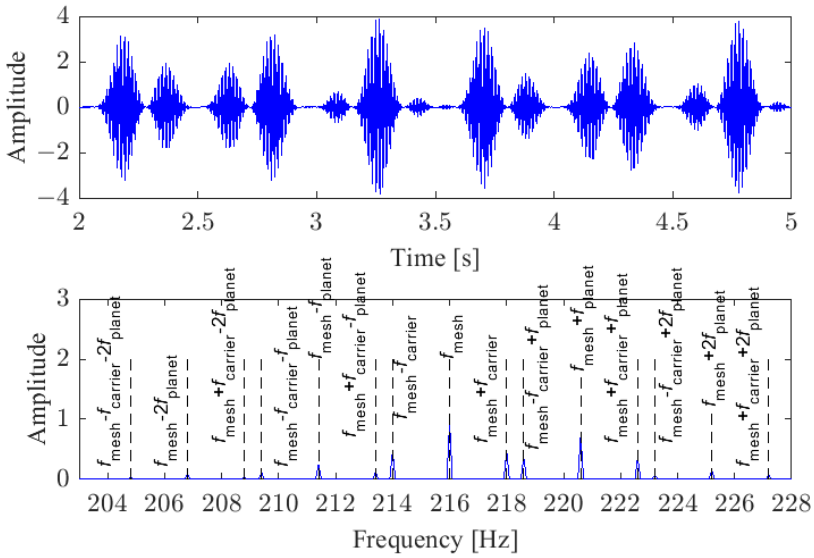

Figure 12. Simulated waveform and Fourier spectrum for a signal for planet gear damage, including the effect of rotation of the planet carrier.

5. Experimental Signal Analysis

In this study, the root cause of vibrations in a planetary gearbox derive the vibration signal model of amplitude modulation (AM) and frequency modulation (FM) due to gear damage and determine the characteristic frequencies of vibrations for a planetary gearbox in Sections 3 and 4. The general procedure for the proposed method is shown in Figure 13, and the basic steps are described as follows.

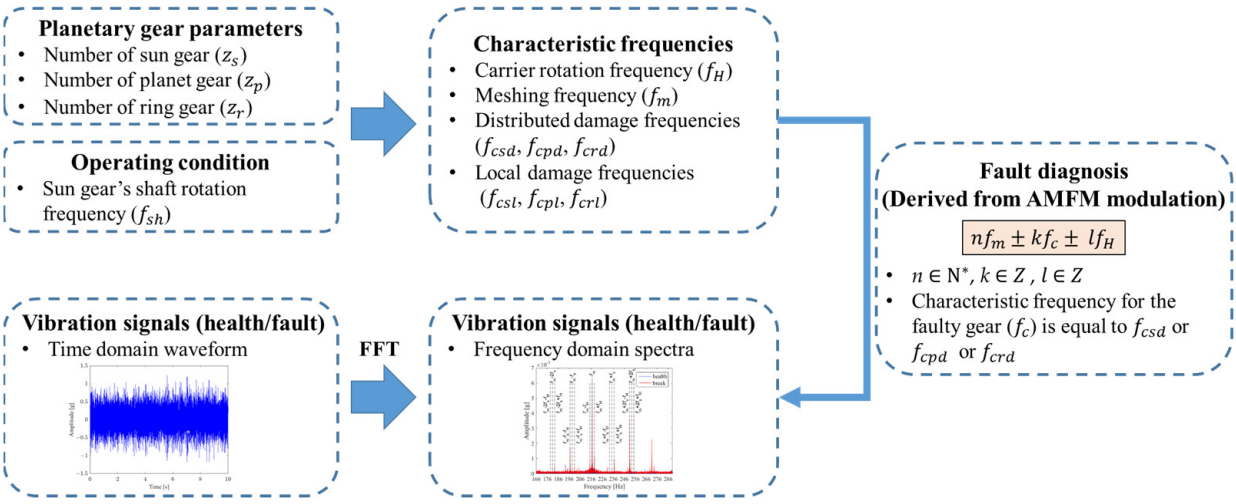

Figure 13. Illustration of the proposed fault diagnosis.

Step 1: Understand the design parameters and operating conditions of the planetary gearbox, such as the number of gear teeth and input speed.

Step 2: Calculate the characteristic frequencies using Equations (11)–(18).

Step 3: Record health and fault vibration signals, which can be represented by time domain waveform signals. Convert time domain waveform signals into frequency domain spectra signals through the fast Fourier transform.

Step 4: The fault diagnosis in the vibration condition of the faulty gear can be verified by AMFM modulation and experimental results. Characteristic frequencies (f_c) and the rotation frequency of the planet carrier (f_H) directly reflect this mechanical modulation

behavior, especially the sideband around the gear meshing frequency (f_m) and its harmonics. This behavior is consistent with the result using Equation (10).

5.1. Test Rig and Planetary Gearbox

The experimental data are for a planetary gearbox test rig at the Industrial Technology Research Institute (ITRI). The configuration of the test rig is shown in Figure 14.

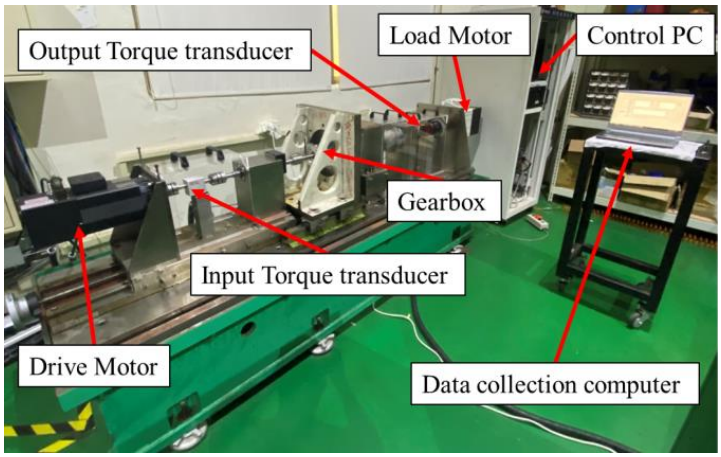

Figure 14. Planetary gearbox test rig.

The experimental set-up consists of a 4.2 kW servo motor on the drive side, a torque transducer on the input and output sides and a 9.4 kW servo motor on the load side that is controlled by a PC. The experiments use a planetary gearbox, and the rotational speeds are 1200, 2100 and 3000 rpm using different loads, as shown in Table 3. The embedded sensor data are acquired by a data collection computer at a sampling frequency of 10 kHz and a sampling time of 180 s.

Table 3. Parameters for the experiment process.

Drive Motor Speed (rpm)	Load Motor (N-m)
1200/2100/3000	32/56/80

Figure 15 shows a schematic diagram of the planetary gearbox. The sun gear is fixed on the shaft as the high-speed input and the planet carrier is the low-speed output. The geometric parameters for the planetary gearbox are listed in Table 4.

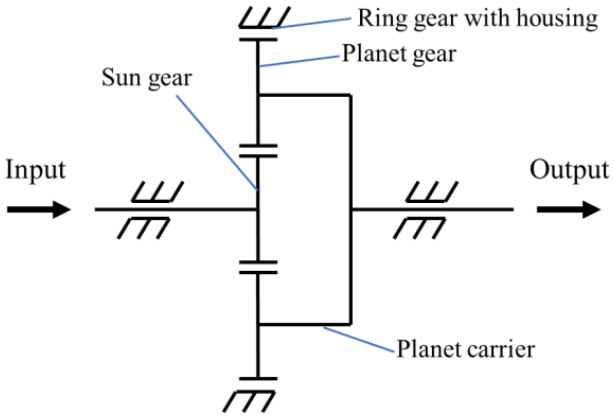

Figure 15. Planetary gearbox diagram.

Table 4. Parameters for the planetary gearbox.

Sun Gear Teeth Number	Planet Gear Teeth Number	Ring Gear Teeth Number	The Number of Planet Gears
12	47	108	3

Figure 16 shows the faulty gear. The fault is artificially manufactured. For each faulty gear scenario, 9 groups of data are recorded using the specified rotational speeds and loads. Each experiment uses a faulty gear, but all other gears are normal.

(**a**) (**b**) (**c**)

Figure 16. Different faulty gear in the gearbox: (**a**) sun gear; (**b**) planet gear; (**c**) ring gear.

As shown in Table 5, when the shaft frequency is determined, the other characteristic frequencies are calculated using Equations (11)–(18). The vibration data are for rotation speeds of 20 Hz (1200 rpm), 35 Hz (2100 rpm) and 50 Hz (3000 rpm) for the test rig.

Table 5. Values of characteristic frequencies (Hz).

Meshing Frequency	Rotating Frequency		Distributed Damage			Local Damage		
	Sun	Carrier	Planet	Sun	Ring	Planet	Sun	Ring
216	20	2	4.6	18	2	4.6	54	6
378	35	3.5	8	31.5	3.5	8	94.5	10.5
540	50	5	11.5	45	5	11.5	135	15

5.2. Comparison of an Accelerometer and an Embedded Sensor

To verify the accuracy of the embedded sensor, the gearbox housing contains a commercially available wired accelerometer as a vibration reference index, as shown in Figure 17. The wired accelerometer specifications are shown in Table 6.

The spectrum for the three-axis vector measurement is not significantly different for the Y direction, so a planetary gearbox with sun gear wear is used, and the test rig uses an input drive motor at 1200 rpm and a load motor at 80 N-m.

The gearbox is run for a time and a segment of vibration signal is collected. Figure 18 shows the time domain and frequency spectrum for the signal in the wired accelerometer and the embedded sensor. The signal for the wired accelerometer has a larger amplitude than that for the embedded sensor, possibly because the wired accelerometer is attached to the surface of the gearbox and the gearbox is sufficiently rigid that the surface amplitude is greater than the amplitude inside. The root mean square (RMS) and peak values are calculated using the time domain signal and are used to determine the condition of the gearbox. The RMS value is 0.258 g, and the peak value is 1.619 g for the wired accelerometer. The RMS value is 0.233 g, and the peak value is 1.393 g for the wireless embedded sensor. These results show that the error in the RMS value is less than 10%, and the error in the peak value is less than 14%. The Fourier spectrum shows that the theoretical meshing frequency for this scenario is 216 Hz, and there is a significant peak in both spectra. The error for the wired accelerometer is 0.032 Hz, and the error for the embedded sensor is 0.861 Hz.

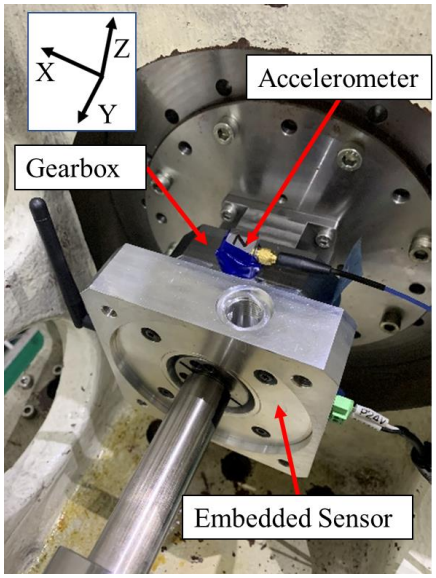

Figure 17. Planetary gearbox sensor locations.

Table 6. Wired accelerometer specifications.

Description	Parameter Value
Model	356A15
Supply Voltage	20 to 30 VDC
Input Range	±50 g
Sensitivity	100 mV/g
Broadband Resolution	0.0002 g rms
Resonant Frequency	>25 kHz

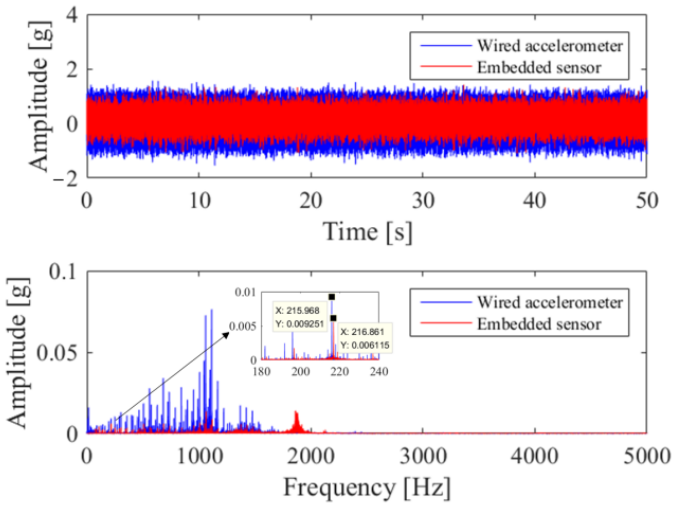

Figure 18. Waveform and Fourier spectrum signal for a wired accelerometer and an embedded sensor.

The time domain and spectrum are similar for the signal in the wired accelerometer and the embedded sensor. Any difference is due to an error in the placement position, the stability of the test rig and the sampling frequency rate difference. The signal analysis for the embedded sensor in the Y direction is used to validate that the spectral analysis can be used to diagnose planetary gearbox faults using the theoretical derivation.

Data are logged on an Internet database file, as shown in Figure 19. When the recording stops, the uploading button is used to run the script to upload the measurement data. An offline analysis uses PC data-log text files or Internet database files.

Date	TimeStep	AccX	AccY	AccZ
2022:08:30:02:06:57.0001	0.0001	0.962806134	0.209391928	0.281872282
2022:08:30:02:06:57.0002	0.0002	1.180247196	0.133096818	0.18268864
2022:08:30:02:06:57.0003	0.0003	1.090600443	-0.000419623	0.039635309
2022:08:30:02:06:57.0004	0.0004	1.247005417	0.056801709	0.04726482
2022:08:30:02:06:57.0005	0.0005	1.048638132	0.127374685	0.14835584
2022:08:30:02:06:57.0006	0.0006	1.002861067	0.014839399	0.26661326
2022:08:30:02:06:57.0007	0.0007	0.947547112	0.016746777	0.270428016
2022:08:30:02:06:57.0008	0.0008	1.042915999	0.14835584	0.150263218
2022:08:30:02:06:57.0009	0.0009	1.12684062	0.199855039	0.049172198
2022:08:30:02:06:57.0010	0.001	1.058175021	0.201762417	0.093041886

Figure 19. Internet database file.

5.3. Sun Gear Fault—Experimental Signal Analysis

Sun gear wear signals are analyzed to verify that the spectral analysis can be used to diagnose faults in planetary gearboxes using the theoretical derivation, and to show the effectiveness with which faults are detected and located for different operating conditions. Artificially seeded wear simulates local gear damage and the spectral peaks are assessed using the characteristic frequency. For all cases, the meshing frequency f_m is dominant at 1200 rpm, and $f_m + 2f_s - f_H$ is dominant at other input speeds.

Figures 20–22 show the time domain waveform and the frequency domain spectra of the wear signals for different input speeds and output loads. The dashed lines show the meshing frequency and the sidebands for the modulation due to planet carrier rotation and sun gear faults. This uses Equation (10). When a tooth on the sun gear is damaged, sidebands appear around the three centers. The sideband spacing is the same as the characteristic frequency for a distributed gear fault.

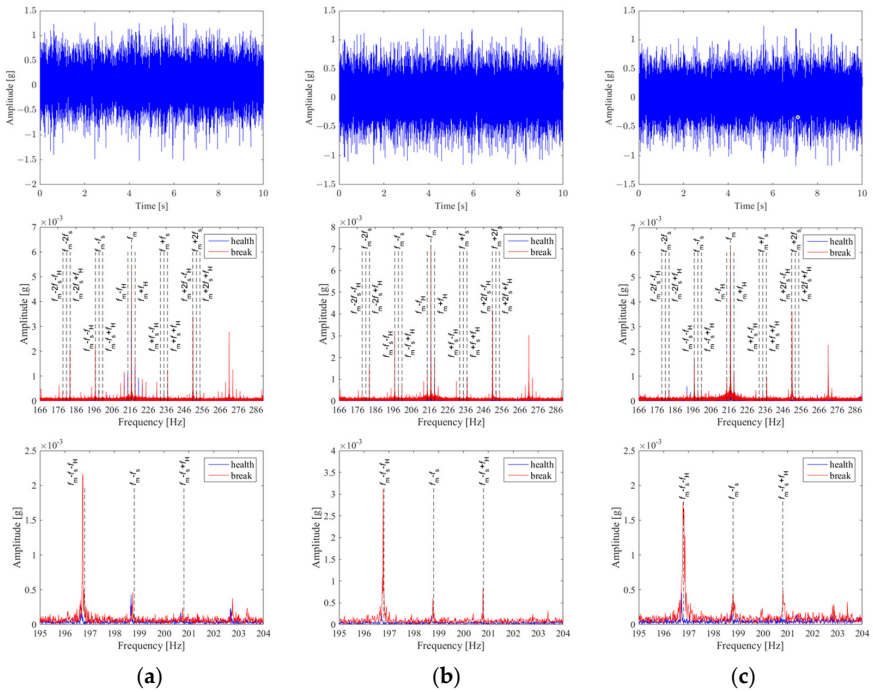

Figure 20. Waveform for a broken sun gear, Fourier spectrum and enlarged Fourier spectrum for an input speed of 1200 rpm and a load of: (**a**) 32 N-m, (**b**) 56 N-m and (**c**) 80 N-m.

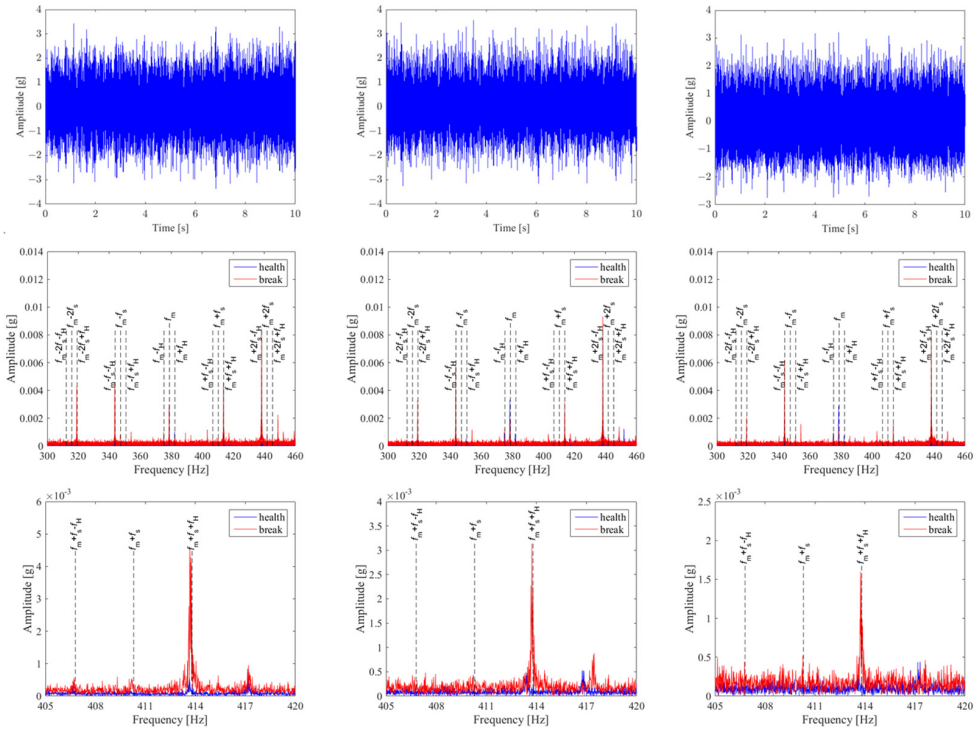

(**a**) (**b**) (**c**)

Figure 21. Waveform for a broken sun gear, Fourier spectrum and enlarged Fourier spectrum for an input speed of 2100 rpm and a load of: (**a**) 32 N-m, (**b**) 56 N-m and (**c**) 80 N-m.

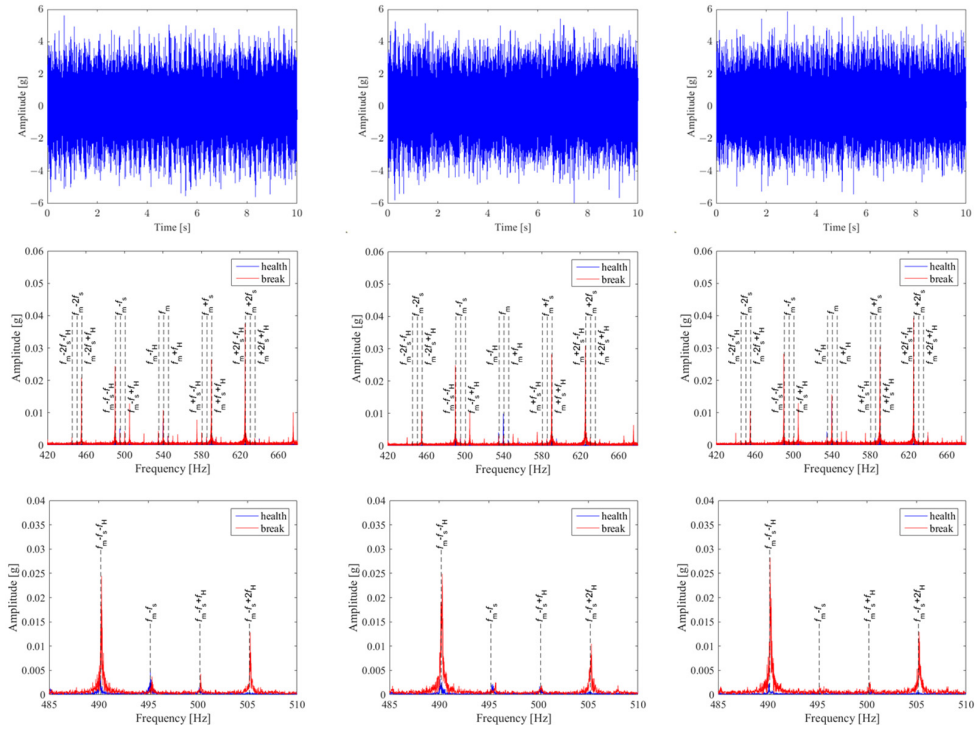

(**a**) (**b**) (**c**)

Figure 22. Waveform for a broken sun gear, Fourier spectrum and enlarged Fourier spectrum for an input speed of 3000 rpm and a load of: (**a**) 32 N-m, (**b**) 56 N-m and (**c**) 80 N-m.

For a health signal, the illustrations show that there are some sidebands at frequencies of $f_m \pm kf_s$ and $f_m \pm kf_s \pm f_H$ (where $k \in Z$), but their amplitude is small. Gear production and gearbox assembly involve errors that result in sidebands, even for normal gears.

Compared to the health signal for 1200 rpm and loads 32 N-m, 56 N-m and 80 N-m, the vibration signal for sun gear wear has different frequency domain spectra, as shown in Figure 20. The spectral peaks occur at the same frequencies of $f_m \pm kf_s$ and $f_m \pm kf_s \pm f_H$ (where $k \in Z$) as those for the health signal. The meshing frequency (f_m) is 216 Hz, the distributed damage frequency of sun gear (f_s) is 18 Hz and the rotating frequency of the planet carrier (f_H) is 2 Hz. The amplitude of the characteristic frequency and the corresponding sidebands increase significantly with sun gear wear, so this study uses sidebands to detect gear faults, rather than the meshing frequency f_m and rotation frequency of the planet carrier minus and plus the meshing frequency $f_m \pm f_H$.

Figure 20 shows an enlarged image of the Fourier spectrum for a wear signal. The sidebands at frequencies of $f_m - f_s - f_H$, $f_m - f_s$ and $f_m - f_s + f_H$ have much larger amplitudes than those for the health signal, so the gearbox is faulty, and the wear is on the sun gear.

For a vibration signal of less than 2100 rpm and loads of 32 N-m, 56 N-m and 80 N-m, the meshing frequency (f_m) is 378 Hz, the distributed damage frequency for the sun gear (f_s) is 31.5 Hz and the rotating frequency of the planet carrier (f_H) is 3.5 Hz. The sidebands at frequencies of $f_m + f_s - f_H$, $f_m + f_s$ and $f_m + f_s + f_H$ have larger amplitudes than those of the health signal, as shown in Figure 21.

For a vibration signal of less than 3000 rpm and loads of 32 N-m, 56 N-m and 80 N-m, the meshing frequency (f_m) is 540 Hz, the distributed damage frequency for the sun gear (f_s) is 45 Hz and the rotating frequency for the planet carrier (f_H) is 5 Hz. The sidebands at frequencies of $f_m - f_s - f_H$ and $f_m - f_s + 2f_H$ have significantly larger amplitudes than those of the health signal, as shown in Figure 22.

5.4. Planet Gear Fault—Experimental Signal Analysis

The effect of planet gear wear on the gearbox is determined using the theoretical derivation. Figures 23–25 show the time domain waveform and the frequency domain spectra of the frequency domain for the health and wear signals for different input speeds and output loads. In all the cases, the frequency component of f_m is dominant, so the frequency for planetary gear is observed in the sidebands in the enlarged Fourier spectrum for the health signal.

Compared to the health signal for 1200 rpm and loads of 32 N-m, 56 N-m and 80 N-m, the signal for the planet gear wear has different frequency domain spectra, as shown in Figure 23. The spectral peaks occur at the same frequencies of $f_m \pm kf_p$ and $f_m \pm kf_p \pm f_H$ (where $k \in Z$) as those for the health signal. The meshing frequency (f_m) is 216 Hz, the distributed damage frequency for the planet gear (f_p) is 4.6 Hz and the planet carrier (f_H) rotational frequency is 2 Hz.

Figure 23 shows the enlarged Fourier spectrum for the wear signal. The sidebands at frequencies of $f_m - 2f_p - f_H$, $f_m - 2f_p$, $f_m - 2f_p + f_H$ and $f_m - f_p$ have much larger amplitudes than those for the health signal, so the gearbox is faulty at the planet gear.

For the vibration signal for a speed of less than 2100 rpm and loads of 32 N-m, 56 N-m and 80 N-m, the meshing frequency (f_m) is 378 Hz, the distributed damage frequency for planet gear (f_p) is 8 Hz and the rotating frequency for the planet carrier (f_H) is 3.5 Hz. The sidebands at frequencies of $f_m + 2f_p + f_H$, $f_m + f_p + f_H$ and $f_m + 2f_p - f_H$ have larger amplitudes than those for the health signal, as shown in Figure 24.

For a vibration signal for a speed of less than 3000 rpm and loads of 32 N-m, 56 N-m and 80 N-m, the meshing frequency (f_m) is 540 Hz, the distributed damage frequency for the planet gear (f_p) is 11.5 Hz and the rotating frequency for the planet carrier (f_H) is 5 Hz. The sidebands at frequencies of $f_m + 2f_p + f_H$ and $f_m + f_p + f_H$ have much larger amplitudes than those for the health signal, as shown in Figure 25.

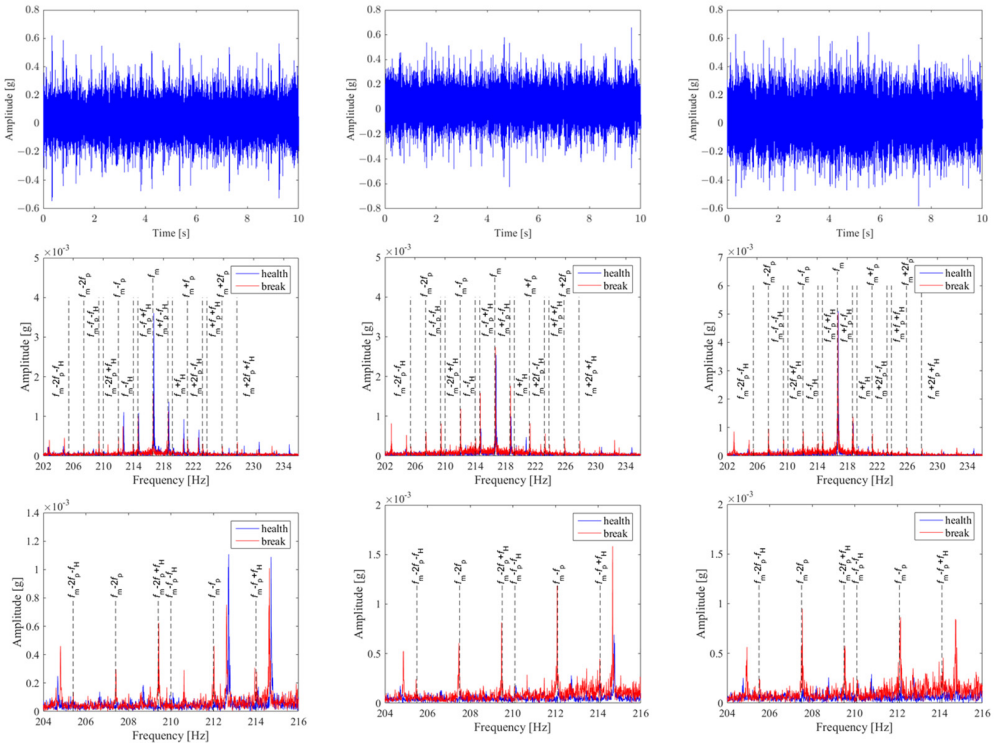

(**a**) (**b**) (**c**)

Figure 23. Waveform for a broken planet gear, Fourier spectrum and enlarged Fourier spectrum for an input speed of 1200 rpm and a load of: (**a**) 32 N-m, (**b**) 56 N-m and (**c**) 80 N-m.

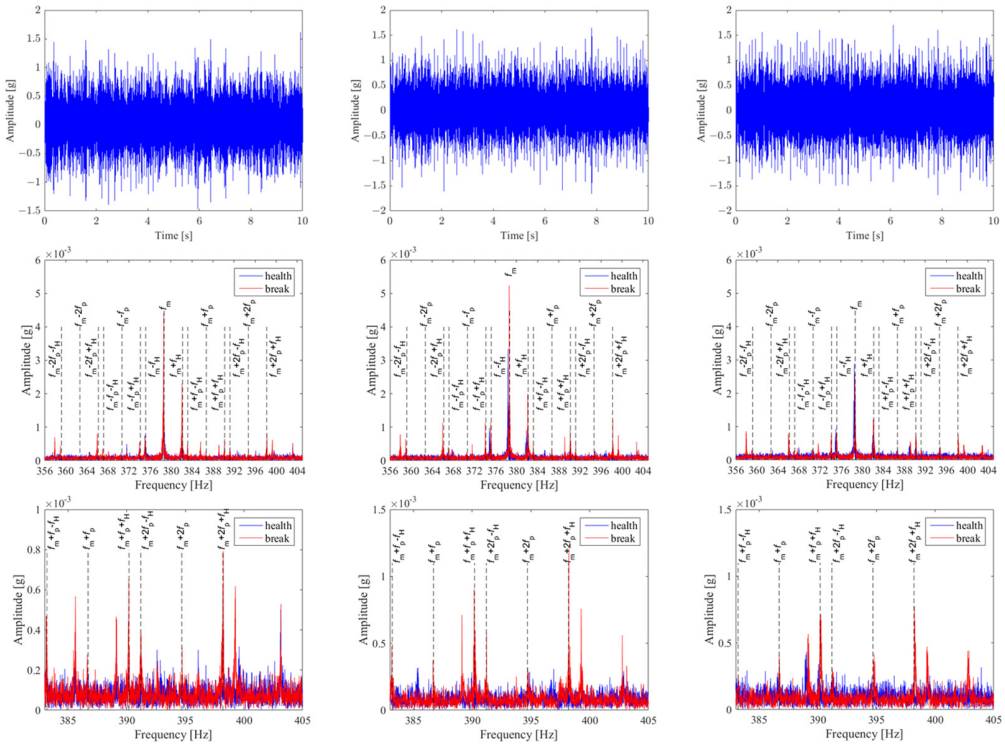

(**a**) (**b**) (**c**)

Figure 24. Waveform for a broken planet gear, Fourier spectrum and enlarged Fourier spectrum at an input speed of 2100 rpm and a load of: (**a**) 32 N-m, (**b**) 56 N-m and (**c**) 80 N-m.

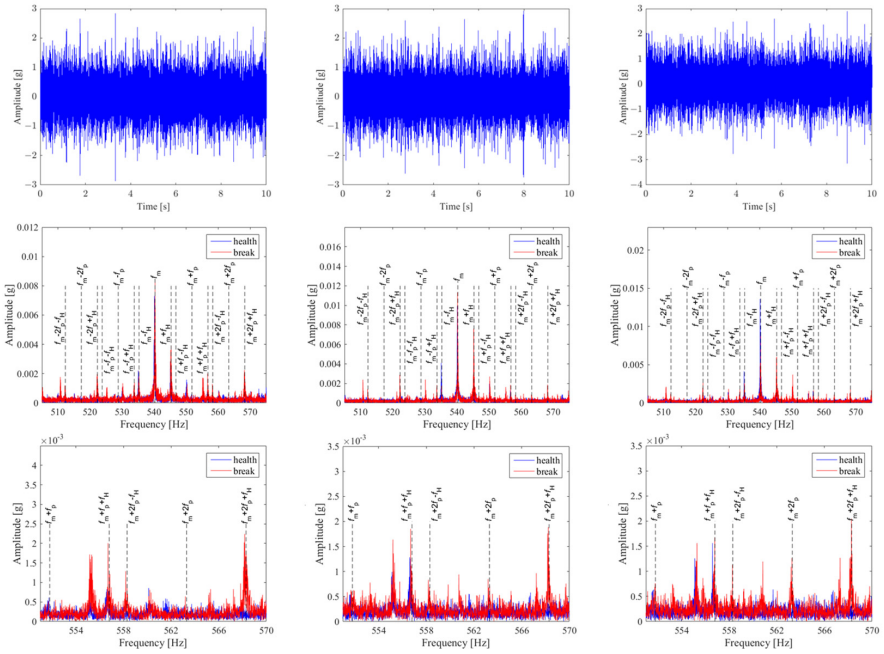

(**a**) (**b**) (**c**)

Figure 25. Waveform for a broken planet gear, Fourier spectrum and enlarged Fourier spectrum at an input speed of 3000 rpm and a load of: (**a**) 32 N-m, (**b**) 56 N-m and (**c**) 80 N-m.

5.5. Ring Gear Fault—Experimental Signal Analysis

The effect of ring gear wear on the gearbox is determined using the theoretical derivation. Figures 26–28 show time domain waveform and the frequency domain spectra of the frequency domain for the health and wear signals for different input speeds and output loads. In all the cases, the frequency component f_m is dominant, so the frequency of planetary gear wear is observed in the sidebands in the enlarged Fourier spectrum for the health signal.

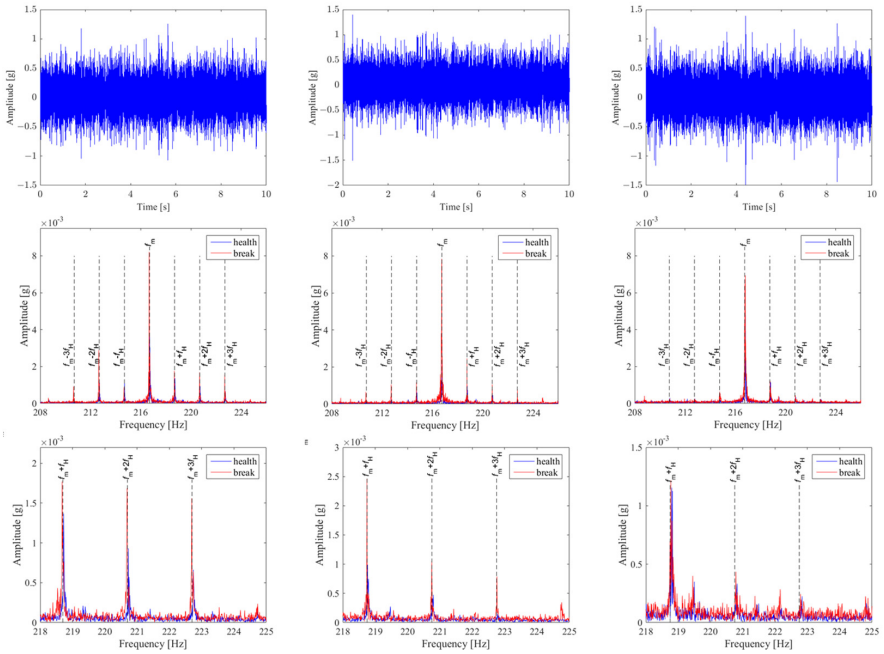

(**a**) (**b**) (**c**)

Figure 26. Waveform for a broken ring gear, Fourier spectrum and enlarged Fourier spectrum for an input speed of 1200 rpm and a load of: (**a**) 32 N-m, (**b**) 56 N-m and (**c**) 80 N-m.

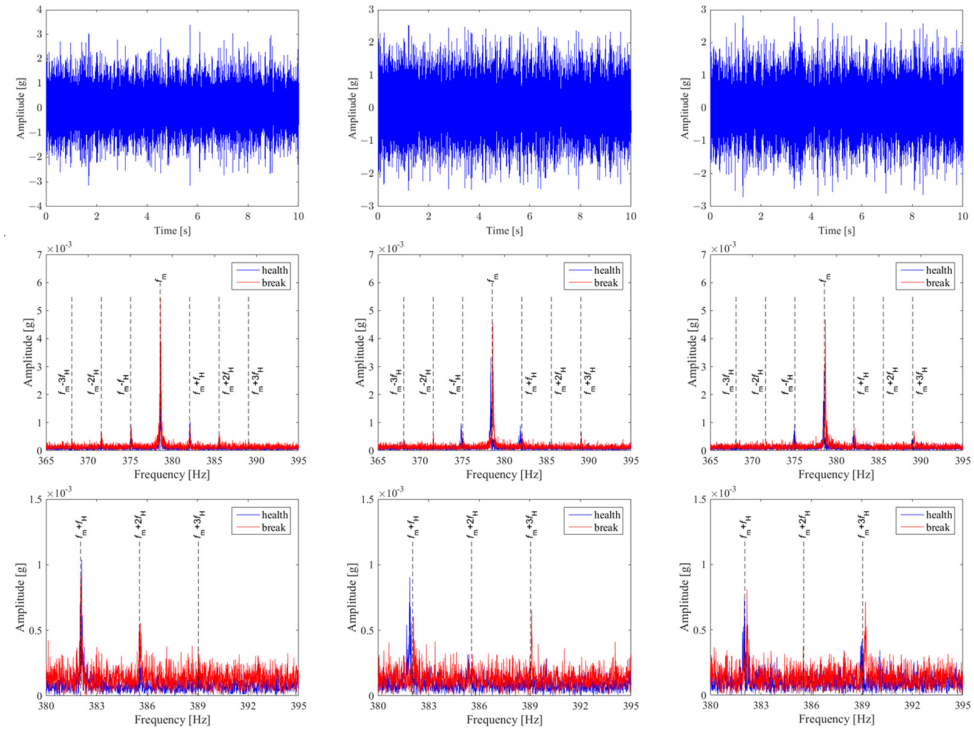

Figure 27. Waveform for a broken ring gear, Fourier spectrum and enlarged Fourier spectrum for an input speed of 2100 rpm and a load of: (**a**) 32 N-m, (**b**) 56 N-m and (**c**) 80 N-m.

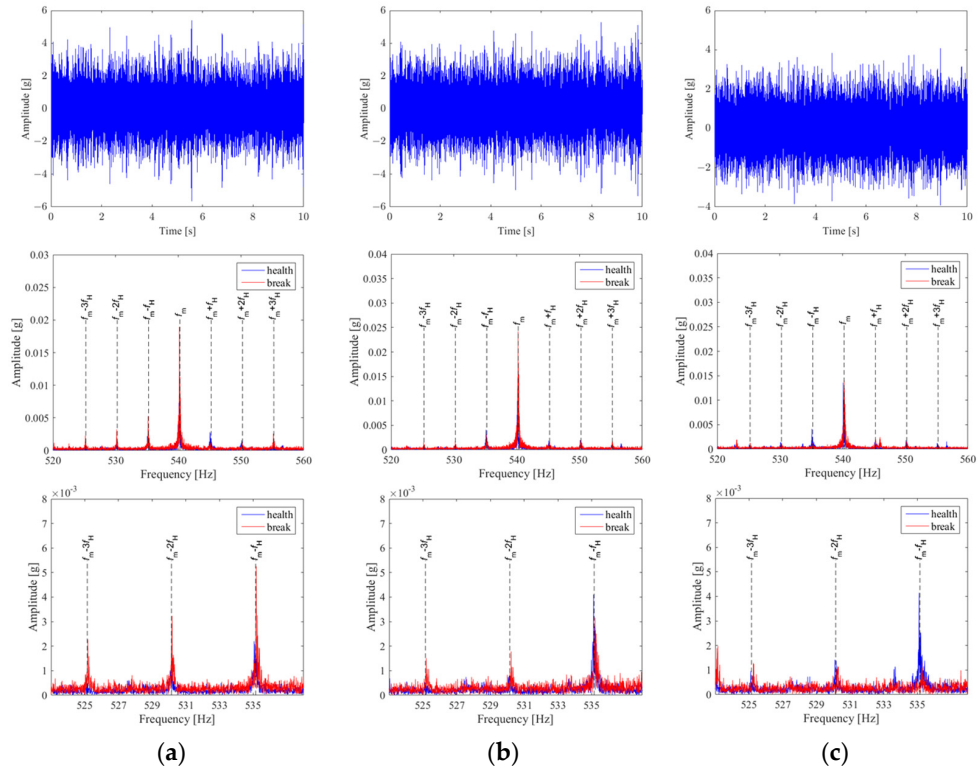

Figure 28. Waveform for a broken ring gear, Fourier spectrum and enlarged Fourier spectrum for an input speed of 3000 rpm and a load of: (**a**) 32 N-m, (**b**) 56 N-m and (**c**) 80 N-m.

Compared to the health signal for 1200 rpm and loads of 32 N-m, 56 N-m and 80 N-m, the meshing frequency (f_m) is 216 Hz and the rotating frequency for the planet carrier (f_H) is 2 Hz. For a vibration signal for 2100 rpm and loads of 32 N-m, 56 N-m and 80 N-m, the meshing frequency (f_m) is 378 Hz and the rotating frequency for the planet carrier (f_H) is 3.5 Hz. For the vibration signal for 3000 rpm and loads of 32 N-m, 56 N-m and 80 N-m, the meshing frequency (f_m) is 540 Hz and the rotating frequency for the planet carrier (f_H) is 5 Hz.

The vibration signal for ring gear wear has different frequency domain spectra, as shown in Figures 26–28. The spectral peaks occur at the same frequencies of $f_m \pm kf_H$ (where $k \in Z$) as those for the health signal. In the enlarged Fourier spectrum for the wear signal, the sidebands at the frequencies of $f_m \pm kf_H$ (where $k \in Z$) have significantly larger amplitudes than those for the health signal, so the gearbox is faulty at the ring gear.

For the experimental signal analysis for faulty gears, there are 9 working conditions, which correspond to different speeds and loads. The results show that the speed has a higher sensitivity to vibration. For the fault frequency, the amplitude of the signals is larger, which validates the theoretical derivations for the vibration signal models and the characteristic frequency for faulty gear in a planetary gearbox.

5.6. Time Domain—Experimental Signal Analysis

In addition to the frequency domain, the time domain signal also verifies the validity of the proposed fault diagnosis vibration model. It is used to calculate the RMS and peak values for the time domain signals for the nine operating conditions. The nine operating conditions' ranges are 1200 rpm from 32 N-m to 80 N-m, 2100 rpm from 32 N-m to 80 N-m and 3000 rpm from 32 N-m to 80 N-m. Figure 29a,b show that the RMS and peak for the sun and ring fault vibration signals are greater than the RMS and peak for the health signals. For the planet gear fault, the RMS and peak values at 1200 rpm are not significantly greater than the health signal, and the peak value at 3000 rpm for loads of 32 N-m and 56 N-m are not greater than the health signal, possibly because there are three planet gears in the gearbox that only has artificially seeded wear, so the impact on the time domain signal is small. In all the experiments, an increase in the input speed causes a stronger vibration, rather than an increase in the output load.

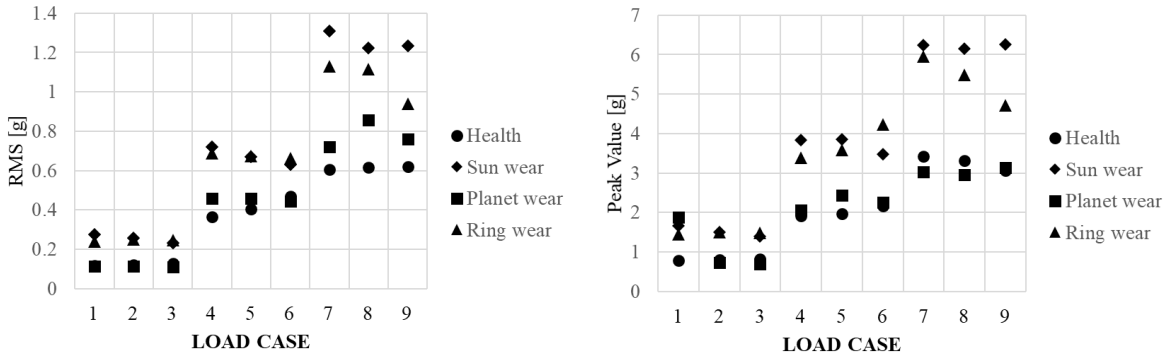

(**a**) (**b**)

Figure 29. Time domain for wear gear for different load cases: (**a**) root mean square (RMS); (**b**) peak value.

Using the time domain quantitative metrics, time domain waveforms and the analysis results in the frequency domain sidebands, gear failures can be detected.

6. Conclusions

Compared with a fixed-shaft transmission system, a planetary gear train has a complex structure and a compound rotational motion mode. This study uses a printed circuit board that integrates temperature and vibration signals from a sensor that is embedded in a planetary gearbox. The signals are transmitted to the server using a wireless module. LabVIEW is used to create a graphical interface that can read the time domain, the frequency

domain and the RMS signals. Vibration signal models are used to detect the planetary gearbox fault and develop reliable fault diagnosis methods.

In terms of the AMFM effect and time variant conditions due to a gear fault, a mathematical model of the vibration signal for a faulty planetary gearbox is established. The characteristic frequencies are calculated to allow the detection and location of faults in the spectrum. Using these theoretical derivations, the time and frequency domains for this proposed model are used to detect planetary gearbox faults.

A planetary gearbox test rig is constructed, and an embedded sensor verifies the validity of the signal model using a wired accelerometer and confirms the results in the time and frequency domains. The vibration data for different operating conditions are measured using the test rig, and the proposed model is verified by manually manufacturing faulty gears. A signal analysis verifies the validity of the signal model and the theoretical equations for the frequency domain spectra and characteristic frequencies of fault gears.

An embedded sensor for a planetary gearbox allows the machine's owner to determine the wear status and when maintenance is required. This reduces the time and money lost due to transmission wear and breakages.

Author Contributions: Conceptualization, L.-T.H.; methodology, L.-T.H.; hardware, L.-T.H.; software, L.-T.H.; validation, L.-T.H.; investigation, L.-T.H.; resources, L.-T.H.; data curation, L.-T.H.; writing—original draft preparation, L.-T.H.; writing—review and editing, J.-Y.C.; visualization, L.-T.H.; supervision, J.-Y.C.; project administration, L.-T.H. All authors have read and agreed to the published version of the manuscript.

Funding: This research was funded by the Industrial Technology Research Institute (ITRI) with grant # M353C92100.

Institutional Review Board Statement: Not applicable.

Informed Consent Statement: Not applicable.

Data Availability Statement: Not applicable.

Conflicts of Interest: The authors declare no conflict of interest.

References

1. Wang, T.; Han, Q.; Chu, F.; Feng, Z. Vibration based condition monitoring and fault diagnosis of wind turbine planetary gearbox: A review. *Mech. Syst. Signal Process.* **2019**, *126*, 662–685. [CrossRef]
2. Zhang, M.; Wang, K.; Li, Y. Motion Periods of Planet Gear Fault Meshing Behavior. *Sensors* **2018**, *18*, 3802. [CrossRef] [PubMed]
3. Lee, H.C.; Chang, Y.C.; Huang, Y.S. A Reliable Wireless Sensor System for Monitoring Mechanical Wear-Out of Parts. *IEEE Trans. Instrum. Meas.* **2014**, *63*, 2488–2497. [CrossRef]
4. Hou, L.; Bergmann, N.W. Novel industrial wireless sensor networks for machine condition monitoring and fault diagnosis. *IEEE Trans. Instrum. Meas.* **2012**, *61*, 2787–2798. [CrossRef]
5. Salvadori, F.; de Campos, M.; Sausen, P.S.; de Camargo, R.F.; Gehrke, C.; Rech, C.; Spohn, M.A.; Oliveira, A.C. Monitoring in Industrial Systems Using Wireless Sensor Network with Dynamic Power Management. *IEEE Trans. Instrum. Meas.* **2009**, *58*, 3104–3111. [CrossRef]
6. Shahzad, K.; Cheng, P.; Oelmann, B. Architecture exploration for a high-performance and low-power wireless vibration analyzer. *IEEE Sens. J.* **2013**, *13*, 670–682. [CrossRef]
7. Peng, Y.; Qiao, W.; Cheng, F.; Qu, L. Wind Turbine Drivetrain Gearbox Fault Diagnosis Using Information Fusion on Vibration and Current Signals. *IEEE Trans. Instrum. Meas.* **2021**, *70*, 3518011. [CrossRef]
8. Wang, C.; Gao, R.X. A virtual instrumentation system for integrated bearing condition monitoring. *IEEE Trans. Instrum. Meas.* **2000**, *49*, 325–332. [CrossRef]
9. Yang, Y.; Ma, H.; Fan, H.; Zhang, C. Design and Test of a Fault Diagnosis System for Planetary Gear Box. In Proceedings of the 2019 International Conference on Sensing, Diagnostics, Prognostics, and Control, Beijing, China, 15–17 August 2019; pp. 862–865.
10. Wang, F.; Zhang, L.; Zhang, B.; Zhang, Y.; He, L. Development of Wind Turbine Gearbox Data Analysis and Fault Diagnosis System. In Proceedings of the 2011 Asia-Pacific Power and Energy Engineering Conference, Wuhan, China, 25–28 March 2011; pp. 1–4.
11. Lin, J.; Dou, C. Design of gearbox fault diagnosis system based on LabVIEW. In Proceedings of the 2010 3rd International Congress on Image and Signal Processing, Yantai, China, 16–18 October 2010; pp. 4206–4208.
12. Lei, Y.; Lin, J.; Zuo, M.J.; He, Z. Condition monitoring and fault diagnosis of planetary gearboxes: A review. *Measurement* **2014**, *48*, 292–305. [CrossRef]

13. Liang, X.; Zuo, M.J.; Hoseini, M.R. Vibration signal modeling of a planetary gear set for tooth crack detection. *Eng. Fail Anal.* **2015**, *48*, 185–200. [CrossRef]
14. Zhang, M.; Zuo, M.J.; Wei, D.; Liu, J.; Wang, K.; Wang, Y. Motion periods of sun gear dynamic fault meshing positions in planetary gear systems. *Measurement* **2020**, *162*, 107897. [CrossRef]
15. McFadden, P.D.; Smith, J.D. An explanation for the asymmetry of the modulation sidebands about the tooth meshing frequency in epicyclic gear vibration. *Proc. Inst. Mech. Eng.* **1985**, *199*, 65–70. [CrossRef]
16. McNames, J. Fourier series analysis of epicyclic gearbox vibration. *J. Vib. Acoust.* **2001**, *124*, 150–152. [CrossRef]
17. Mosher, M. Understanding vibration spectra of planetary gear systems for fault detection. In Proceedings of the ASME Design Engineering Technical Conferences, Chicago, IL, USA, 2–6 September 2003; pp. 645–652.
18. Molina Vicuña, C. Theoretical frequency analysis of vibrations from planetary gearboxes. *Forsch Ing.* **2012**, *76*, 15–31. [CrossRef]
19. Inalpolat, M.; Kahraman, A. A theoretical and experimental investigation of modulation sidebands of planetary gear sets. *J. Sound Vib.* **2009**, *323*, 677–696. [CrossRef]
20. Inalpolat, M.; Kahraman, A. A dynamic model to predict modulation sidebands of a planetary gear set having manufacturing errors. *J. Sound Vib.* **2010**, *329*, 371–393. [CrossRef]
21. Luo, H.; Hatch, C.; Hanna, J.; Kalb, M.; Weiss, A.; Winterton, J.; Inalpolat, M.; Dannehy, C. Amplitude modulations in planetary gears. *Wind Energy* **2014**, *17*, 505–517. [CrossRef]
22. He, G.; Ding, K.; Li, W.; Li, Y. Frequency response model and mechanism for wind turbine planetary gear train vibration analysis. *IET Renewable Power Gener.* **2017**, *11*, 425–432. [CrossRef]
23. Feng, Z.; Zuo, M.J. Vibration signal models for fault diagnosis of planetary gearboxes. *J. Sound Vib.* **2012**, *331*, 4919–4939. [CrossRef]
24. Miao, Q.; Zhou, Q. Planetary Gearbox Vibration Signal Characteristics Analysis and Fault Diagnosis. *Shock Vib.* **2015**, *2015*, 126489. [CrossRef]